JOURNAL OF GEOPHYSICAL RESEARCH, VOL. 113, D16S40, doi:10.1029/2007JD008818, 2008

Click Here for Full Article

Validation of SO_2 retrievals from the Ozone Monitoring Instrument over NE China

Nickolay A. Krotkov,[1] Brittany McClure,[2,3] Russell R. Dickerson,[2,3] Simon A. Carn,[4] Can Li,[5] Pawan K. Bhartia,[6] Kai Yang,[1] Arlin J. Krueger,[4] Zhanqing Li,[5] Pieternel F. Levelt,[7] Hongbin Chen,[8] Pucai Wang,[8] and Daren Lu[8]

Received 15 April 2007; revised 14 November 2007; accepted 16 January 2008; published 18 June 2008.

[1] The Dutch-Finnish Ozone Monitoring Instrument (OMI) launched on the NASA Aura satellite in July 2004 offers unprecedented spatial resolution, coupled with contiguous daily global coverage, for space-based UV measurements of sulfur dioxide (SO_2). We present a first validation of the OMI SO_2 data with in situ aircraft measurements in NE China in April 2005. The study demonstrates that OMI can distinguish between background SO_2 conditions and heavy pollution on a daily basis. The noise (expressed as the standard deviation, σ) is $\sim$1.5 DU (Dobson units; 1 DU = $2.69 \cdot 10^{16}$ molecules/cm^2) for instantaneous field of view boundary layer (PBL) SO_2 data. Temporal and spatial averaging can reduce the noise to $\sigma \sim 0.3$ DU over a remote region of the South Pacific; the long-term average over this remote location was within 0.1 DU of zero. Under polluted conditions collection 2 OMI data are higher than aircraft measurements by a factor of two. Improved calibrations of the radiance and irradiance data (collection 3) result in better agreement with aircraft measurements on polluted days. The air mass–corrected collection 3 data still show positive bias and sensitivity to UV absorbing aerosols. The difference between the in situ data and the OMI SO_2 measurements within 30 km of the aircraft profiles was about 1 DU, equivalent to $\sim$5 ppb from 0 to 3000 m altitude. Quantifying the SO_2 and aerosol profiles and spectral dependence of aerosol absorption between 310 and 330 nm are critical for an accurate estimate of SO_2 from satellite UV measurements.

Citation: Krotkov, N. A., et al. (2008), Validation of SO_2 retrievals from the Ozone Monitoring Instrument over NE China, *J. Geophys. Res.*, *113*, D16S40, doi:10.1029/2007JD008818.

1. Introduction

[2] Sulfur dioxide (SO_2) is a short-lived gas, produced primarily by volcanoes, power plants, refineries, metal smelting and burning of fossil and biofuels. It can be a noxious pollutant or a major player in global climate forcing, depending on altitude. Most fossil fuel burning occurs near the surface where SO_2 is released into the planetary boundary layer (PBL). When SO_2 remains near the Earth's surface, it has detrimental health and acidifying effects but exerts little impact on global climate or radiative forcing. Emitted SO_2 is soon converted to sulfate aerosol by reaction with OH in air or by reaction with H_2O_2 in aqueous solutions (clouds) [*Seinfeld and Pandis*, 1998; *Chin et al.*, 2000]. The mean lifetime varies from $\sim$1–2 days or less near the surface to more than a month in the stratosphere [e.g., *Krueger et al.*, 2000; *Benkovitz et al.*, 2004]. The resulting sulfate aerosol, which can be transported distantly in the free troposphere, can have climate effects, including direct radiative forcing and aerosol-induced changes in cloud microphysics. The concentration and lifetime of SO_2, the meteorological mechanisms that loft it above the PBL, and the efficiency of those mechanisms remain major unanswered questions in global atmospheric chemistry and climate science [e.g., *Dickerson et al.*, 2007].

[3] Emission inventories indicate that the largest increases in tropospheric SO_2 emissions have occurred in Asia during the last 20 years [*Streets and Waldhoff*, 2000; *Streets et al.*, 2003; *Larssen et al.*, 2006; *Ohara et al.*, 2007]. These increased emissions resulted in a positive winter trend (17% per decade) in sulfate aerosol loading over Asia between 1979 and 2000 detected by the NASA Total Ozone Mapping Spectrometer (TOMS) instrument [*Massie et al.*, 2004]. The TOMS aerosol trend is consistent with a pronounced regional increase in aerosol optical

[1]Goddard Earth Sciences and Technology Center, University of Maryland, Baltimore County, Baltimore, Maryland, USA.
[2]Department of Chemistry, University of Maryland, College Park, Maryland, USA.
[3]Also at Department of Atmospheric and Oceanic Sciences, University of Maryland, College Park, Maryland, USA.
[4]Joint Center for Earth Systems Technology, University of Maryland, Baltimore County, Baltimore, Maryland, USA.
[5]Department of Atmospheric and Oceanic Sciences, University of Maryland, College Park, Maryland, USA.
[6]Laboratory for Atmospheres, NASA Goddard Space Flight Center, Greenbelt, Maryland, USA.
[7]Royal Netherlands Meteorological Institute, De Bilt, Netherlands.
[8]Institute of Atmospheric Physics, Chinese Academy of Sciences, Beijing, China.

Copyright 2008 by the American Geophysical Union.
0148-0227/08/2007JD008818$09.00

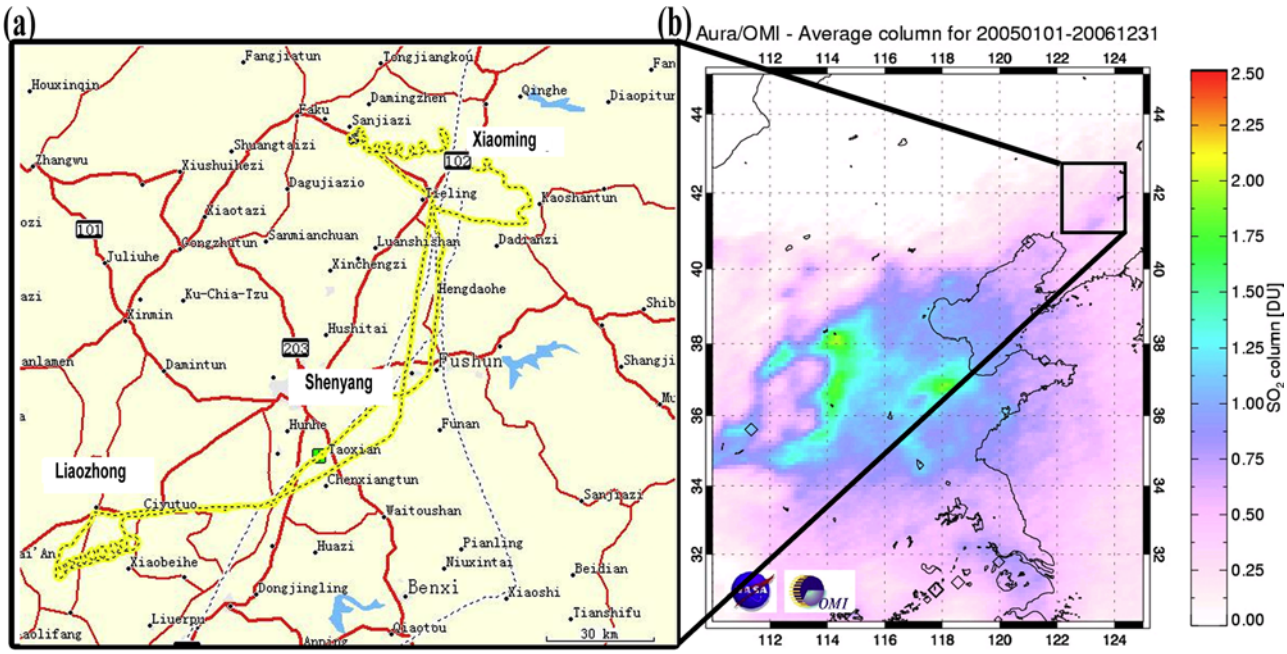

Figure 1. (left) Flight path on 5 April 2005. Aircraft profiling flight patterns (spirals) were performed near Xiaoming (42.45°N, 123.7°E) and Liaozhong (41.35°N, 122.648°E). All flights departed from Taoxian International Airport (41.640°N, 123.488°E) in the Liaoning region of China. Flight paths were similar on 5, 7 and 10 April 2005. (http://www.atmos.umd.edu~zli/EAST-AIRE/air_camp/air_camp.htm). (right) A 2-year average OMI SO_2 map over eastern China in Dobson units (1 DU = $2.69 \cdot 10^{16}$ molecules/cm^2) showing persistent areas of high SO_2 concentrations in a triangle between Beijing, Shanghai, and the Sichuan basin in agreement with emission inventories [*Streets and Waldhoff*, 2000; *Streets et al.,* 2003; *Larssen et al.*, 2006; *Ohara et al.*, 2007]. Smaller SO_2 enhancements (~0.5 DU) over the Shenyang region in northeast China (black square) are significant as compared to the background regions.

thickness over coastal areas of Asia detected using Advanced Very High Resolution Radiometer (AVHRR) satellite data [*Mishchenko and Geogdzhayev*, 2007]. However, no historic satellite data are available for estimating trends in anthropogenic SO_2 emissions over the same period. The TOMS sensitivity to SO_2 was limited by the available instrument wavelengths and low spatial resolution (~50 km at nadir and ~100 km average) to large SO_2 amounts in volcanic eruptions [*Krueger et al.*, 1995, 2000; *Carn et al.*, 2003] and exceptional SO_2 pollution events [*Carn et al.*, 2004]. Greatly improved sensitivity was demonstrated through the detection of volcanic and anthropogenic SO_2 in full-spectrum UV data provided by the Global Ozone Monitoring Experiment (GOME) [*Eisinger and Burrows*, 1998; *Burrows et al.*, 1999; *Thomas et al.*, 2005; *Khokhar et al.*, 2005] and Scanning Imaging Absorption Spectrometer for Atmospheric Cartography (SCIAMACHY) [*Bovensmann et al.*, 1999; *Bramstedt et al.*, 2004; *Richter et al.*, 2006]. However, GOME needs 3 days and SCIAMACHY 6 days to acquire a contiguous global map and hence could miss short-lived pollution events. The Ozone Monitoring Instrument (OMI) [*Levelt et al.*, 2006] launched on NASA's Aura satellite [*Schoeberl et al.*, 2006] in July 2004 offers better spatial resolution (13 × 24 km at nadir), coupled with contiguous global daily coverage, for space-based UV measurements of SO_2. OMI SO_2 data are publicly available from NASA's Goddard Space Flight Center Earth Sciences (GES) Data and Information Services Center (DISC) at http://disc.sci.gsfc.nasa.gov/Aura/OMI/omso2_v003.shtml. By using optimum wavelengths, the retrieval sensitivity is improved over TOMS by factors of 10 to 20, depending on location [*Krotkov et al.*, 2006]. The ground footprint of OMI is one eighth the area of TOMS [*Levelt et al.*, 2006]. These factors produce a two orders of magnitude improvement in the minimum detectable mass of SO_2. The improved OMI sensitivity permits daily observations of strong anthropogenic SO_2 emissions (from smelters and coal burning power plants) [*Krotkov et al.*, 2006, 2007; *Carn et al.*, 2007]. These retrievals require validation against independent measurements.

[4] In situ profile measurements by low-altitude aircraft are important for validating satellite SO_2 retrievals and for providing critical information about vertical profiles of gases (SO_2, ozone) and aerosols in the PBL. Although such measurements are available for several years over the eastern U.S. [*Taubman et al.*, 2006], no data were previously available over China. Here we present the first comparisons of the OMI SO_2 retrievals with in situ aircraft measurements near Shenyang in NE China (Figure 1) [*Dickerson et al.*, 2007]. Aircraft and OMI PBL SO_2 data sets are briefly discussed in section 2 together with error estimates. Parameterization of the air mass factor (AMF) is suggested to improve the accuracy of the operational OMI data. Section 3 describes aircraft comparisons with opera-

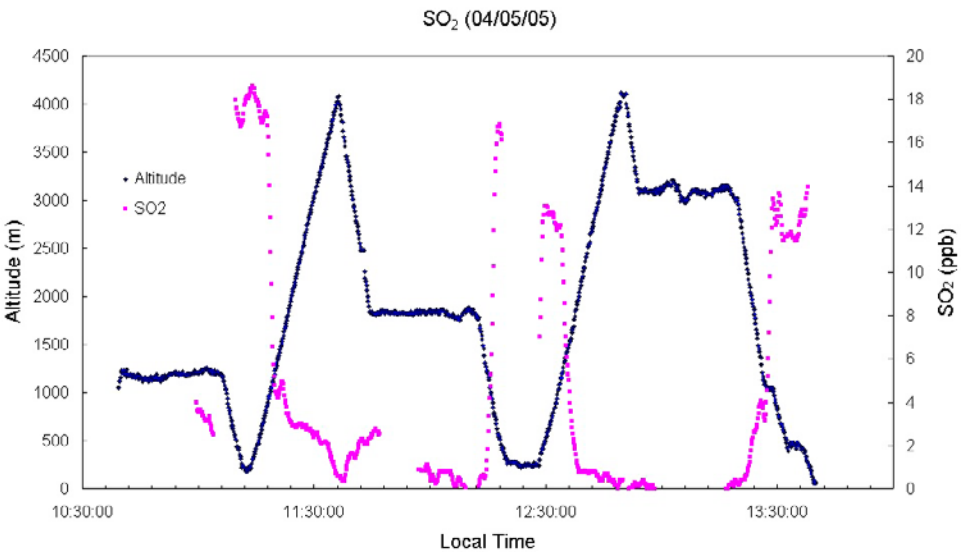

Figure 2. Altitude (blue) and in situ SO_2 (red) aircraft data as function of flight time (local time (LT): LT = UT + 8 h) on 5 April 2005 over northeastern China (Figure 1). The amount of SO_2 increases as the altitude decreases during the flight. These raw data were converted into three SO_2 vertical profiles over Liaozhong (1130 LT) and Xiaoming (1230 LT) and on the descent to Taoxian International airport (1330 LT). The OMI overpass time (0457 UT) corresponds to 1257 LT.

tional OMI PBL SO_2 data for 4 days in April 2005 with different meteorological and air quality conditions. Several improvements to the operational OMI SO_2 data are discussed including new OMI radiance and irradiance calibrations (collection 3) and off-line AMF corrections based on aircraft measurements of altitude profiles of SO_2 and aerosols.

2. Data Collection

2.1. Aircraft Data

[5] The aircraft measurements were performed as part of the East Asian Study of Tropospheric Aerosols: an International Regional Experiment (EAST-AIRE) [*C. Li et al.*, 2007; *Z. Li et al.*, 2007]. Eight flights were completed between 1 April 2005 and 12 April 2005. Only 4 days with different air quality and meteorological conditions (1, 5, 7 and 10 April) were selected for comparisons because of the optimal OMI observational conditions (no clouds, near nadir viewing directions). All flights departed from Taoxian International Airport (41.640°N, 123.488°E) in the Liaoning province of China. Flight paths were similar on 5, 7 and 10 April (Figure 1). Two profiling flight patterns (spirals) were performed daily over farmland, from ~300 m up to 4,000 m above sea level (asl) to the south (Liaozhong) and north (Xiaoming) of the airport (Figure 1). The flight on 1 April was in a north-south direction (to Harbin) with only one measured SO_2 profile on the descent to the Taoxian International Airport. The flights were made on a Chinese Y-12 twin-engine turboprop plane. Two inlets were located on top of the cockpit in front of the engines: a forward facing isokinetic inlet to collect aerosols and a backward facing inlet for trace gas measurements. All instruments on board have been used on previous flights over the eastern U.S. [*Taubman et al.*, 2006] and are well characterized [*Dickerson et al.*, 2007]. SO_2 was measured using a commercially modified pulse-florescence detector with a detection limit of about 0.2 ppbv and an estimated absolute accuracy of ~15% (95% confidence level) [*Luke*, 1997]. The contributions to this uncertainty include sampling line loss, instrument noise, and interference by other species. Relative humidity and temperature were measured with a solid-state probe (EIL Instruments Inc., Rustrak RR2–252, Hunt Valley, MD) and pressure was monitored with a Rosemount Model 2005 Pressure Transducer. Location was monitored with a Global Positioning System receiver (Garmin GPS-90). The temperature and pressure measurements (accurate to 1%) were used to convert the SO_2 mixing ratio to absolute concentration. The concentrations measured during each spiral were extrapolated to the surface and vertically integrated below the maximum aircraft altitude (~4 km) to estimate SO_2 column amounts with an overall uncertainty of ~20% for column contents above ~0.3 DU. Other instruments on board have been previously described in more detail [*Taubman et al.*, 2006; *Dickerson et al.*, 2007]. Aerosol scattering coefficients at three wavelengths (450, 550, and 700 nm) were measured with an integrating nephelometer (TSI Model 3563) [*Anderson et al.*, 1996]. The nonideal forward scattering truncation was corrected following *Anderson and Ogren* [1998]. The aerosol optical thickness (AOT) and Angstrom coefficient were estimated from the measured scattering coefficients assuming a constant single scattering albedo (SSA) of ~0.9. The Angstrom coefficient was biased high and AOT was biased low compared to coincident ground-based AERONET observations because of insufficient sampling of large dust particles. The estimated bias was ~20% for anthropogenic pollution (when fine particles dominate), but could increase to 50–100% during dust storms (when coarse particles dominate).

[6] Figure 2 shows typical aircraft SO_2 data as a function of flight time (local time (LT): LT = UT + 8 h) on 5 April.

Table 1a. OMI Instantaneous Field of View (IFOV) SO_2 Noise Statistics Over Background Regions in the South Pacific on 6 April 2005 (OMI Collection 2 Operational Data, Orbit 3858)

Sample Area	Number of IFOV Data	Area Mean SO_2 Column Content, DU	Standard Deviation of IFOV Data, DU
41–43°S; 130–132°E	105	−0.2	1.4
40–44°S; 128–134°E	594	−0.05	1.5
Whole orbit from 70°S to 30°N	47684	0.02	1.4

On that day, high concentrations of SO_2 (~10 ppbv) and aerosols (scattering coefficients $\sim 4 \cdot 10^{-4}$ m^{-1}) were observed within the PBL, below 1000 m asl. Above the PBL, pollutant levels dropped rapidly with altitude, but were still substantial compared to background levels, with SO_2 close to 1 ppbv and aerosol scattering coefficients close to 10^{-4} m^{-1} above 2000 m asl.

2.2. OMI SO_2 Data

[7] In the publicly released OMI SO_2 product (OMSO2) four reported total SO_2 values correspond respectively to the a priori profile assumptions of SO_2 in the PBL (below 2 km) and in the lower troposphere from anthropogenic sources, SO_2 distributed between 5 and 10 km emitted by passive volcanic degassing in the free troposphere, and SO_2 distributed between 15 and 20 km representing injection from explosive volcanic eruptions. The PBL data are processed with the Band Residual Difference (BRD) algorithm [*Krotkov et al.*, 2006], while all other data are processed with the Linear Fit (LF) algorithm [*Yang et al.*, 2007]. Both algorithms use the TOMS–like total ozone retrieval (OMTO3) [*Bhartia and Wellemeyer*, 2002] as a linearization step to derive an initial estimate of total ozone (assuming zero SO_2) and the wavelength-independent Lambertian effective surface reflectivity (LER). The OMTO3 algorithm accomplishes this by matching calculated radiances to the measured radiances at a pair of wavelengths (317.5 nm and 331.2 nm under most conditions). The residuals at the 10 other wavelengths are then calculated as the difference between the measured and computed N values ($N = -100 * log_{10}(I/F)$, I is Earth radiance and F is solar irradiance), where the latter account for the effects of multiple Rayleigh scattering, ozone absorption, Ring effect, and surface reflectivity. In the presence of SO_2, the residuals contain spectral structures that correlate with the SO_2 absorption cross sections. The residuals also have contributions from other error sources. To reduce this interference, a median residual for a sliding group of SO_2-free and cloud-free pixels covering ±15° latitude along the orbit track is subtracted for each spectral band and cross-track position [*Yang et al.*, 2007]. This "sliding median" empirical correction essentially acts as a high-pass filter forcing median residuals to equal zero for all the bands. Doing so, any cross-track and latitudinal biases are reduced.

[8] Only operational OMI PBL data, processed with the BRD algorithm, will be discussed in this paper. The algorithm uses differential residuals at the three wavelength pairs with the largest differential SO_2 cross sections in the OMI UV2 spectral region (310–380 nm) to maximize measurement sensitivity to anthropogenic emissions in the PBL. Each pair residual is converted to SO_2 slant column density (SCD) using differential SO_2 cross-section data at constant temperature (275 K) [*Bogumil et al.*, 2003]. The SCDs of the three pairs are averaged and the average SCD is converted to the total SO_2 vertical column density (VCD) in Dobson units, (1 DU = $2.69 \cdot 10^{16}$ molecules/cm^2), using a constant air mass factor (AMF) of 0.36:

$$total\ SO_2\ VCD = \frac{SCD}{AMF} \tag{1}$$

[9] This operational AMF was estimated for cloud- and aerosol-free conditions, using a solar zenith angle of 30°, nadir viewing direction, a surface albedo of 0.05, a surface pressure of 1013.3hPa, a 325 DU midlatitude ozone profile [*McPeters et al.*, 2007] and a typical summer SO_2 vertical profile over the eastern U.S. [*Taubman et al.*, 2006].

2.2.1. OMI SO_2 Precision

[10] An estimate of the OMI SO_2 precision (noise) and detection limit can be obtained by examining the retrieval statistics over pristine oceanic regions, where SO_2 amounts

Table 1b. Statistics for the Area-Averaged SO_2 Noise in the South Pacific Region (41–43°S; 130–132°E) on 6 April 2005 (OMI Collection 2 Operational Data, Orbit 3858)

Averaging Radius, km	Average Number of IFOV, n	Average of the Area Means (DU)	Standard Deviation of the Area Means (SDM), n	$\frac{StdDev(IFOV)}{\sqrt{n}}$
20	4	−0.23	0.82	0.73
30	8	−0.22	0.62	0.48
40	14	−0.22	0.51	0.36
50	22	−0.22	0.44	0.29
60	32	−0.21	0.39	0.24
70	44	−0.20	0.36	0.21
80	57	−0.18	0.33	0.18
90	72	−0.16	0.31	0.16
100	89	−0.16	0.28	0.15

Table 1c. Temporal Statistics of the Daily Area Mean OMI PBL SO_2 Values From 2005 Over a Background Region in the South Pacific and Over the EAST-AIRE Flight Region in NE China[a]

Location	Region	Number of Days	Annual Mean, DU	Standard Deviation, DU	Percent Outliers Outside ±2 St Dev
South Pacific	41–43°S, 130–132°E	75	−0.01	0.6	7%
NE China	41–43°N, 122–124°E	110	0.65	1.1	6%

[a]Only days with at least 70 cloud-free IFOV retrievals were used. The long-term average SO_2 column content of 0.65 DU is equivalent to about 3 ppb in the lowest 2 km of the atmosphere over NE China.

are indistinguishable from zero (<0.1 DU) [*Seinfeld and Pandis*, 1998; *Chin et al.*, 2000]. Because of measurement and retrieval errors the OMI Instantaneous Field of View (IFOV) SO_2 data have a statistical distribution in such background regions. The random noise plus spatial variability and temporal variability should explain all the variance in the IFOV data. If the retrieved OMI SO_2 signal is due to random fluctuations such as detector noise then the variability should decrease as the time for which the signal is averaged (and the area over which the signal is averaged) increases. The uncertainty in the average column content should decrease with the square root of the number of IFOV observations averaged (n). For example, consider a region in the South Pacific Ocean bounded by 40–44°S and 128–134°E on 6 April 2005 (Table 1a). This region was chosen because of the absence of SO_2 emissions, and similar observational conditions to the EAST-AIRE region (same orbit, same viewing geometry, absence of clouds). Table 1a shows that both the mean and standard deviation (σ = 1.5 DU) of the IFOV data do not change with the size of the averaging area, so the region is spatially homogeneous. Assuming Gaussian noise statistics, each IFOV SO_2 retrieval is expected to be within +/−3 DU (2σ) in ~95% of cases. This noise level is too high to detect background SO_2 amounts or most anthropogenic SO_2 [*Taubman et al.*, 2006]. Therefore, spatial smoothing is recommended to reduce the noise (i.e., averaging all IFOV data within certain radius for a given location). The standard deviation of the means of the areas (SDM) can be taken as an estimate of the smoothed noise. Table 1b shows the smoothed noise statistics over the same area on 6 April. As the number of averaged IFOV data (n) increases with the averaging radius, the SDM decreases, but more slowly than $StdDev(IFOV)/\sqrt{n}$. For example, the OMI noise in 30 km averages (n = ~8) is estimated to be 0.6 DU, while taking 100 km averages (n = ~90) would reduce the noise to ~0.3 DU. Taking into account large day-to-day variability in area mean values even over pristine locations (Table 1c), we double the OMI noise estimate to account for the temporal noise component. The OMI detection limit is therefore ~3 DU for IFOV data (±two StdDev(IFOV)), but reduces to ~1.2 DU (±four SDM(n), n = ~90, Table 1b) for daily 100 km averages. Time-averaging further reduces the noise, enabling detection of weaker stationary SO_2 emissions not obvious in daily data (Figure 1). The long-term (1 year) mean over the S. Pacific region is zero with a standard deviation of

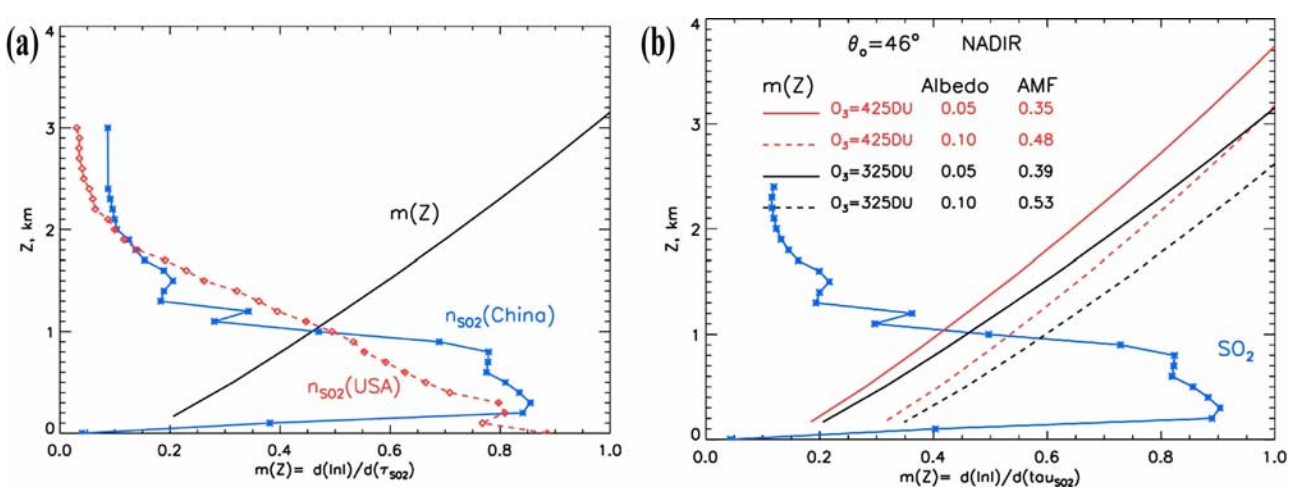

Figure 3. (left) SO_2 vertical profiles: measured during EAST-AIRE campaign on 5 April 2005 over Liaozhong, NE China (blue stars); median summer SO_2 profile over eastern U.S. [*Taubman et al.*, 2006] (red diamonds). Both SO_2 profiles are dimensionless, normalized to a unit column SO_2 amount. Black line shows vertically resolved OMI SO_2 sensitivity or local AMF: $m(z, R_S, \Omega, \theta, \theta_0, \phi)$ calculated for nadir viewing direction ($\theta = 0°$), solar zenith angle $\theta_0 = 46°$, surface reflectivity R_S, = 0.05, Ω = 325 DU middle latitude TOMS climatological ozone profile, no aerosols and clouds. (right) Local AMF dependence on surface albedo, R_S (solid line, $R_S = 0.05$; dashed line, $R_S = 0.1$) and total ozone, Ω (red indicates TOMS Ω = 425 DU midlatitude ozone profile and black indicates Ω = 325 DU midlatitude ozone profile).

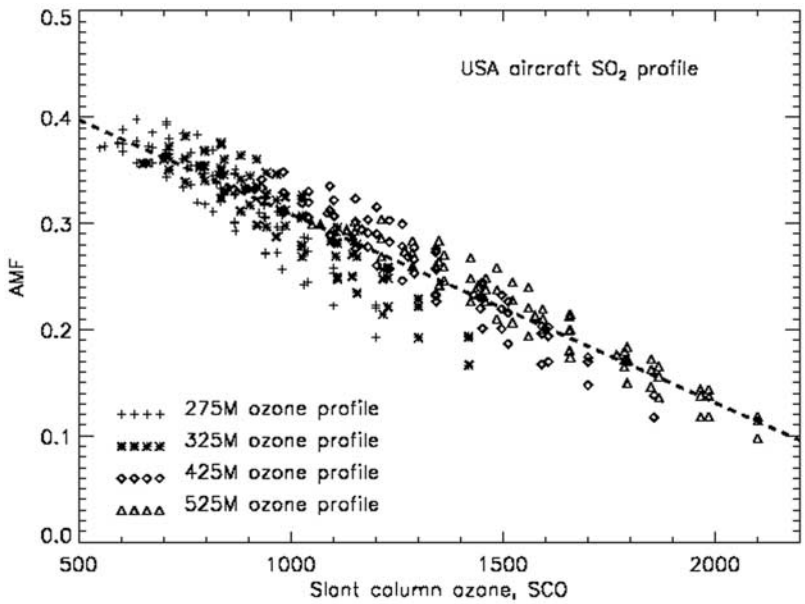

Figure 4. AMF parameterization as function of slant column ozone amount (SCO): $SCO = \Omega \cdot (\sec(\theta) + \sec(\theta_0))$ in Dobson units. The parameterization was calculated using the median summer SO_2 profile measured by aircraft over the eastern U.S. [*Taubman et al.,* 2006], TOMS climatological middle latitude ozone profiles, different viewing angles (0–60°), solar zenith angles (0–60°), and relative solar azimuth angles (60–120°) and a surface albedo of 0.05 with no aerosols or clouds. Dashed line is the linear regression (6) $AMF = r_0 - r_1 \cdot SCO$, where $r_o = 0.486$ and $r_1 = 0.000177$ [DU]$^{-1}$.

~0.6 DU, while over NE China the long-term mean value is 0.65 DU with a standard deviation ~1.1 DU (Table 1c). These results illustrate persistent SO_2 emissions over NE China (Figure 1).

2.2.2. OMI SO_2 Accuracy

[11] The SO_2 retrieval accuracy depends on the uncertainty in both SCD, ε_{SC}, and in average photon path, characterized by the error in assumed AMF: ε_{AMF} (1). The combined error, ε_{SO_2}, can be expressed using equation (1) and assuming that ε_{SC} and ε_{AMF} are not correlated:

$$\frac{\varepsilon_{SO_2}}{\Xi} = \sqrt{\left(\frac{\varepsilon_{SC}}{SCD}\right)^2 + \left(\frac{\varepsilon_{AMF}}{AMF}\right)^2} \tag{2}$$

where Ξ is the total SO_2 VCD, $SCD = 0.36 \cdot \Xi$ (1), and ε_{SC} is estimated from the background noise statistics (ε_{SC} = ~0.2 DU or ~$6 \cdot 10^{15}$ molecules/cm^2 for a 2° by 2° area). The ε_{SC} error has additional systematic components due to uncertainties in laboratory measured SO_2 cross sections [*Bogumil et al.*, 2003] and the algorithmic assumption of a constant PBL temperature. Assuming that the effective PBL temperature ranges from 260 K to 300 K, the operational OMI PBL SO_2 values, derived by assuming a constant effective temperature of 275 K, are overestimated by 4% or underestimated by 8% at these two extremes. This error should be corrected off-line if SO_2 and temperature profiles are known from ancillary measurements or models (see section 3.2). The AMF error, ε_{AMF}, is systematic and increases with deviation of the observational conditions from those assumed in the operational algorithm. For a quantitative use of PBL SO_2 data (i.e., emissions estimates), the operational AMF should be corrected to account for actual observational conditions. Given the relatively high noise in SCD values (30–50% for EAST-AIRE regional averages (Table 2) and up to 200% for the individual pixels (Table 3)), the AMF correction does not need to be exact. Here, we propose a simple parameterization that can be used to estimate the AMF with ~20% uncertainty using only OMI measurements of total ozone.

2.2.3. AMF Parameterization

[12] The AMF depends on SO_2 vertical profile, surface albedo (R_S), observational geometry (viewing (θ), solar zenith (θ_0) and relative solar azimuth (φ) angles), total column ozone (Ω), aerosols and clouds:

$$AMF = \int_0^\infty m(z, R_S, \Omega, \theta, \theta_0, \varphi) n_{SO_2}(z) dz \tag{3}$$

$$m(z) = \frac{\partial \ln(I_{TOA})}{\partial \tau_{SO2}(z)} \tag{4}$$

where $m(z, R_S, \Omega, \theta, \theta_0, \varphi)$ is the vertically resolved OMI SO_2 sensitivity (i.e., local AMF), I_{TOA} is the OMI measured reflectance at the top of atmosphere, $\tau_{SO2}(z)$ is the SO_2 absorption optical thickness in a vertical layer between z [km] and z + dz [km], and $n_{SO2}(z)$ is the dimensionless normalized SO_2 vertical profile shape (Figure 3). Since $m(z)$ is weakly dependent on wavelength, we consider spectrally averaged value over a narrow spectral window (i.e., 311–315 nm) used by the OMI BRD algorithm [*Krotkov et al.*, 2006]. Figure 3 compares the summer median SO_2 profile measured over the eastern U.S. [*Taubman et al.*, 2006] with

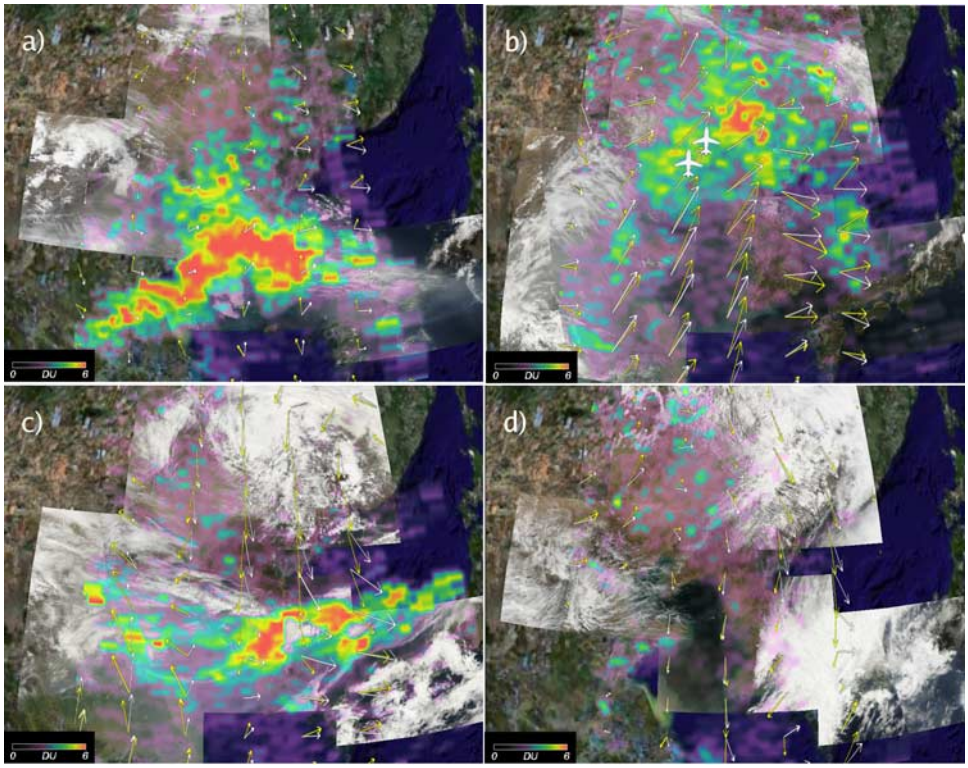

Figure 5. Aura OMI PBL SO2 maps (linear color scale from 0 to 6 DU) superimposed on Aqua MODIS RGB images (images courtesy of MODIS Rapid Response Project at NASA/GSFC) acquired 15 min prior to the OMI overpass during the EAST-AIRE field campaign on (a) 1 April, (b) 5 April (polluted air seen over NE China ahead of the a cold front), (c) 7 April (polluted air pushed off the coast), and (d) 10 April (behind cold front) 2005. The aircraft spiral locations are denoted by white aircraft symbols in Figure 5b. Apparently high SO_2 values (red colors) indicate SO_2 lofting above the PBL and/or above low-level clouds, where OMI sensitivity is enhanced. Tropospheric winds are indicated by yellow (surface) and white (850 mbar) arrows. Background maps are from Google Earth screen captures (Google Earth imagery © Google Inc., used with permission) containing imagery from TerraMetrics, Inc. (Copyright 2008 TerraMetrics, Inc., http://www.truearth.com).

a profile measured over NE China during the EAST-AIRE campaign in April 2005. Both SO_2 profiles are normalized to a unit column SO_2 amount. Thus, the AMF can be interpreted as a profile-weighted mean value of the vertically resolved OMI SO_2 sensitivity, $m(z)$ (4). Although the typical SO_2 profile shapes are quite different for the eastern U.S. and China, it turns out that the profile-integrated AMF is close to ~0.4 in both cases. Therefore, AMF corrections due to the measured SO_2 profile shape for EAST-AIRE conditions are expected to be small. Increasing the surface albedo from 0.05 to 0.1 increases the AMF by ~35% (Figure 3, right). However, the land albedo is typically small at UVB wavelengths (310–315 nm), so using the default value (R_S = 0.05) will result in less than a 15% AMF error. A large increase in total ozone from 325 DU to 425 DU causes only a 10% decrease in the AMF, but this systematic effect can be easily taken into account using the OMI total ozone measurements.

$$SO_2(corrected) = \frac{0.36}{AMF(corrected)} SO_2(operational) \quad (5)$$

[13] The AMF correction due to observational geometry (θ, θ_0, φ) can be combined with the total ozone correction using a simple linear regression with respect to the slant column ozone (SCO) (Figure 4):

$$AMF(corrected) = r_0 - r_1 \cdot SCO \quad (6)$$

$$SCO = \Omega \cdot (\sec(\theta) + \sec(\theta_0)) \quad (7)$$

where Ω is the total column ozone measured by OMI. The regression coefficients, r_0 and r_1 depend on the shape of the SO_2 vertical profile, the surface albedo, azimuth angle and the presence of aerosols and clouds. Figure 4 compares parameterized AMF values calculated using the regression (5)–(7) with values calculated with the forward radiative transfer model [*Dave*, 1964] for different ozone profiles and observational geometries. The operational AMF of 0.36 is underestimated by 20% for SCO < 700 DU (Ω = ~300 DU, small solar zenith and viewing angles), but overestimated by ~30% for SCO = 1500 DU. For larger SCO values (high ozone and/or high solar zenith and viewing angles, mostly at high latitudes), the AMF becomes very small, so valid

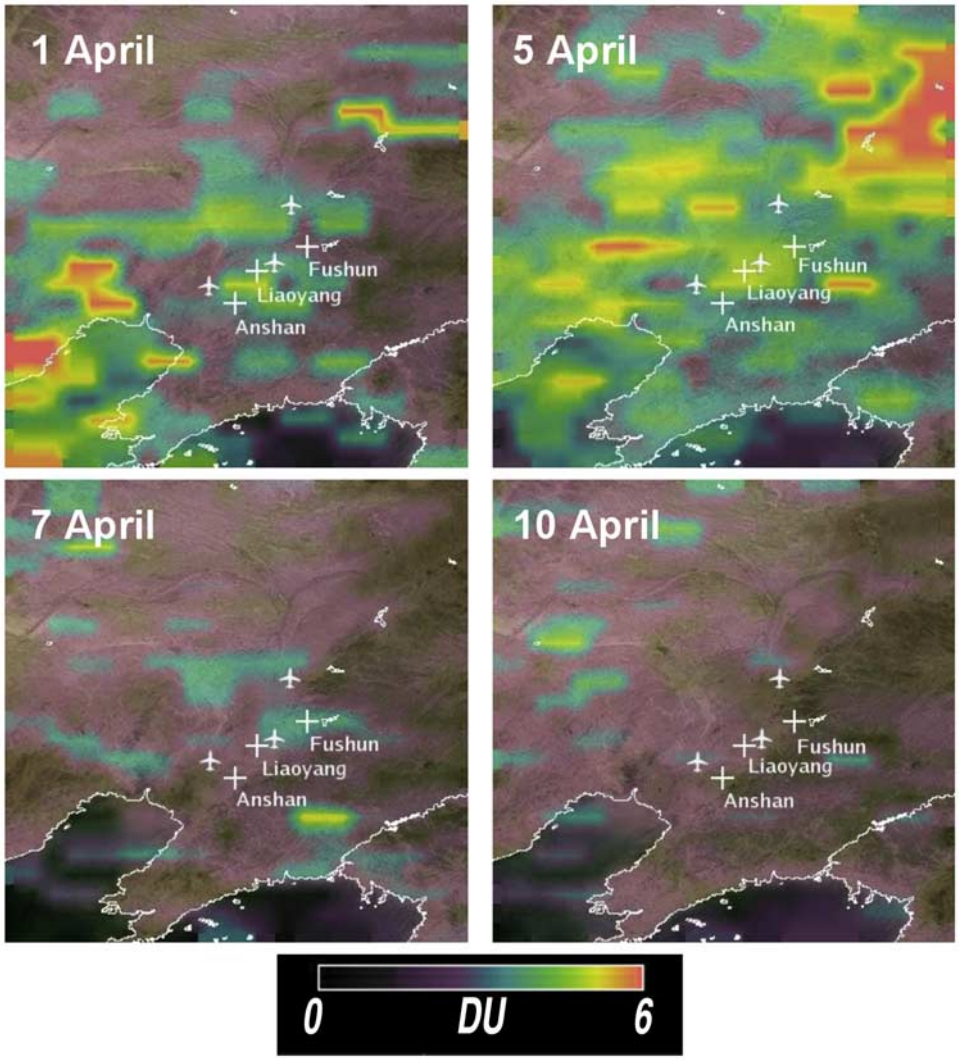

Figure 6. Operational (collection 2) OMI PBL SO_2 data over the EAST-AIRE flight region in April 2005. Background maps are from Google Earth screen captures (Google Earth imagery © Google Inc., used with permission) containing imagery from TerraMetrics, Inc. (Copyright 2008 TerraMetrics, Inc., http://www.truearth.com). MODIS image courtesy of MODIS Rapid Response Project at NASA/GSFC.

PBL SO_2 retrievals are not expected. The parameterization (6) does not account for AMF dependence on relative satellite-solar azimuthal angle, φ. Because of the OMI polar sun-synchronous afternoon orbit (1345 local equator crossing time), φ ranges between 0° and 30° for cross-track positions 1–30, but φ is ~150–180° for positions 31–60 in the tropics. In the middle to high latitudes φ approaches 60–120°. The AMF typically decreases as φ increases from 0°

Table 2. OMI and Aircraft SO_2 Column Density Averaged Over the EAST-AIRE Flight Region in April 2005[a]

Day	Number IFOV, n	OMI Collection 2 Data: Ozone, DU (SD)	LER (SD)	AI (SD)	SO_2, DU (SD)	OMI Collection 3: SO_2, DU (SD)	Aircraft Column SO_2,[b] DU
1 Apr	74	399 (4)	0.06 (0.01)	1.8 (0.2)	2.1±0.7[c] (1.4)	1.4±0.7[d] (1.5)	1.3±0.3
5 Apr	113	367 (4)	0.08 (0.01)	2.1 (0.2)	2.9±0.6 (1.2)	1.9±0.6 (1.2)	1.7±0.3
7 Apr	98	342 (3)	0.05 (0.02)	2.8 (0.6)	0.9±0.6 (1.4)	0.9±0.6 (1.3)	0.1±0.1
10 Apr	90	382 (5)	0.09 (0.05)	0.9 (0.3)	0.45±0.6 (1.2)	0.5±0.6 (1.1)	0.09±0.1

[a]Also shown are OMI regional average ozone (DU), aerosol index (AI) and reflectivity (LER) from the OMTO3 algorithm. The variability over the flight region (one standard deviation) is shown in parentheses. The high AI recorded on 7 April 2005 suggests that mineral dust at altitudes above those flown by the aircraft may create a positive interference.

[b]Vertically integrated (from the surface to 4 km) in situ SO_2 profile averaged over all spirals.

[c]Standard deviation of the area mean SO_2 retrievals with comparable IFOV sample size (n) over a background area in the South Pacific (Table 1b) multiplying by factor of 2 to account for day-to-day variability (Table 1c) and not including AMF error.

[d]Collection 3 noise statistics are the same as collection 2.

to 180°, so in extreme cases a 20% error is possible. However, averaging regression coefficients for φ in the range 60–120° reduces the error to +/−10%. Therefore, under cloud- and aerosol-free conditions the remaining AMF error should be within 20%, less than the noise in SCD values. However, aerosols and clouds can affect the error differently depending on many factors. The assumption is that clouds screen PBL SO_2, but no AMF correction is attempted to account for this "hidden" SO_2. To avoid this uncertainty, only cloud-free days are considered for validation, so that OMI area-weighted reflectivity (LER) is less than 0.1. The aerosol AMF corrections are further discussed in section 4.

3. OMI SO_2 Validations

[14] Figure 5 shows operational OMI PBL SO_2 values combined with high-resolution MODIS RGB composites on the 4 days in April 2005 selected for validation: 1, 5, 7 and 10 April. The MODIS instrument is aboard the EOS Aqua polar orbiting satellite [*King et al.*, 2003], which orbits the Earth 15 min ahead of Aura along the same orbit. According to high-resolution MODIS imagery, the flight region (i.e., 41–43°N and 122–124°E) was cloud-free on all days as confirmed by low average OMI reflectivity (LER < 0.1; Table 2). However, air quality was dramatically different on these days because of different meteorological regimes. Between 5 and 7 April and 9 and 10 April cold fronts traveled from continental China over Korea to the Sea of Japan. Polluted SO_2-rich air was "pushed" ahead of the cold fronts and lofted above the PBL. Mostly cloud-free and SO_2-free air was behind the cold fronts. For example, the location of the cold front on 7 April could be clearly identified in both MODIS imagery and OMI SO_2 maps (Figure 5c). Apparently high OMI operational SO_2 values (>5 DU) over Korea and SE China on 1 and 7 April provide evidence of polluted air lofting above the PBL, where OMI SO_2 sensitivity increases (Figure 3). Since the PBL OMI data are not corrected for the SO_2 lofting effect, the operational values are overestimates. When an elevated SO_2 plume travels above low-level meteorological clouds, the OMI sensitivity is enhanced because of cloud reflection (Figure 3) and additional overestimation results. Therefore, for elevated plumes, off-line correction is needed to account for both SO_2 plume height and underlying cloud reflectivity. Estimating the SO_2 amount for elevated plumes in the lower free troposphere (below 5 km) needs special consideration and is the subject of future studies. In this paper, we only consider OMI data over the EAST-AIRE flight region (41–43°N and 122–124°E) where SO_2 was located predominantly in the PBL, as confirmed by aircraft in situ profile measurements (Figure 2).

3.1. Area Average Comparisons

[15] Figure 6 shows smoothed operational OMI SO_2 data over the EAST-AIRE flight region on the comparison days. Qualitatively, OMI measurements of SO_2 agree with the aircraft in situ observations of high concentrations of SO_2 (approximately 1–2 DU) ahead of the cold front (1 and 5 April) and lower concentrations behind it (7 and 10 April). This comparison demonstrates that OMI can distinguish between background SO_2 conditions and heavy pollution on a daily basis. Quantitatively, there are definite differences between the aircraft and OMI measurements averaged over

Table 3. Comparisons Between Aircraft Spirals and OMI IFOV SO_2 Measurements Averaged Within 30 km of Each Spiral[a]

				OMI[c]						
		Aircraft[b]		Collection 3 SO_2, DU		Collection 2[d]				
Day 2005	Spiral Location and Start Time, UT	τ_{aer} (500)[e]	SO_2, DU	AMF Corrected[f]	Operational[g]	SO_2, DU	n	O_3, DU	AI	LER
1 Apr	Xiaoming, N/A	N/A	no data	N/A	0.7 ± 1.4	1.9	6	395	1.6	0.07
1 Apr	Taoxian 0723	0.5[h]	1.3 ± 0.2	2.1 ± 1.6	1.4 ± 1.6	2.7	4	403	1.7	0.06
1 Apr	Liaozhong, N/A	N/A	no data	N/A	1.1 ± 1.4	1.5	6	404	2.1	0.07
5 Apr	Xiaoming 0429	1.19	1.3 ± 0.2	1.6 ± 1.3	1.5 ± 1.3	2.6	7	367	2.0	0.07
5 Apr	Taoxian 0517	0.64	1.5 ± 0.3	2.7 ± 1.2	2.8 ± 1.2	3.8	9	371	2.1	0.07
5 Apr	Liaozhong 0312	1.11	2.3 ± 0.4	2.5 ± 1.2	2.4 ± 1.2	2.7	8	367	2.4	0.09
7 Apr	Xiaoming 0735	0.56	0.0 ± 0.1	N/A[i]	0.8 ± 1.2	1.1	8	342	3.6	0.04
7 Apr	Taoxian 0920	0.43	0.22 ± 0.1	1.2 ± 1.3	1.5 ± 1.3	1.6	7	342	2.5	0.04
7 Apr	Liaozhong 0857	0.41	0.0 ± 0.1	N/A[i]	1.5 ± 1.4	1.3	6	341	4.3	0.02
10 Apr	Xiaoming 0257	0.23	0.07 ± 0.1	0.5 ± 1.4	0.6 ± 1.4	0.7	6	385	1.0	0.12
10 Apr	Taoxian 0453	0.17	0.21 ± 0.1	0.9 ± 1.3	0.7 ± 1.3	0.5	7	381	0.7	0.14
10 Apr	Liaozhong 0428	0.15[j]	0.04 ± 0.1	0.6 ± 1.3	0.6 ± 1.3	0.5	7	376	0.8	0.10

[a]n is the number of IFOV data averaged. Spiral locations were 42.450°N, 123.70°E (Xiaoming, 138 m asl) and 41.35°N, 122.648°E (Liaozhong, 15 m asl). All flights departed from Taoxian International Airport (41.640°N, 123.488°E, 58 m asl) in the Shenyang region.

[b]Aircraft in situ measured SO_2 concentrations were extrapolated to the surface and vertically integrated up to the maximal aircraft altitude ~4 km to estimate SO_2 column densities with an uncertainty of ~20%.

[c]OMI IFOV data were averaged within 30 km of each spiral location.

[d]OMI operational collection 2 data: ozone, aerosol index (AI) and reflectivity collection 2 data from the OMTO3 algorithm [*Bhartia and Wellemeyer*, 2002].

[e]Aerosol optical thickness (AOT) at 500 nm was estimated from aircraft in situ measurements of aerosol scattering coefficients at 450 nm, 550 nm and 650 nm and integrated from the surface up to 4 km assuming a SSA of 0.9 at 500 nm.

[f]Collection 3 SO_2 data with temperature and AMF corrections applied.

[g]Reprocessed OMI data using the operational SO_2 algorithm with recalibrated radiance and irradiance (collection 3 level 1b) data [*Dobber et al.*, 2008].

[h]On 1 April aircraft measurements were taking during a quick descent to the airport, so that aerosol AOT data are less reliable (nephelometer's averaging time is 5 min). The AOT was obtained from a ground-based handheld Sun photometer. The observation time of the Sun photometer is about 0230–0500 UTC and the OMI overpass was at 0522 UTC.

[i]The aircraft in situ measurements over Xiaoming and Liaozhong on 7 April suggest almost no SO_2 throughout the whole column covered by the aircraft.

[j]The aircraft aerosol data were affected by flying through a deck of fair weather cumulus clouds. Ground-based AERONET aerosol optical thickness data from near the Liaozhong site (41°30′N and 122°42′E) on 10 April were used.

the flight region on both clean and polluted days as shown in Table 2. On clean days 7 and 10 April the aircraft vertically integrated in situ SO_2 measurements (~0.1 DU) were below the OMI detection limit (~1 DU). The disagreement between aircraft and satellite observations could originate from a layer of SO_2 in the upper troposphere or lower stratosphere. There is no way to rule out high concentrations of SO_2 above the maximum flight altitude (4000 m), although this is unlikely. The difference between these days is that the 5–6 April cold front brought with it large amounts of desert dust as confirmed by a high OMI aerosol index (AI) on 7 April (AI = ~3; Table 2), while the AI value was low on 10 April, suggesting no dust. Dust aerosols typically have a strong absorption enhancement in the shorter UVB wavelengths [*d'Almeida et al.*, 1991; *Sokolik and Toon*, 1999; *Alfaro et al.*, 2004] and could interfere with OMI SO_2 retrievals. The dust interference is a subject of future study.

[16] As opposed to clean days, 1 and 5 April represent polluted air masses ahead of cold fronts (Figure 5). Trajectory analysis [*Draxler and Rolph*, 2003] suggests that the air on 1 April was from the northwest at 500, 1000, and 2000 m above ground level (Figure 5a). The local meteorological records at Taoxian airport indicate weak winds with variable directions on that day. The trajectories on 5 April are mainly from the southwest. Before reaching the Shenyang area, the air passed over many emission sources in major industrial regions, including the Beijing [*An et al.*, 2007] and Shanghai areas. Aircraft measurements on 5 April show high SO_2 concentrations throughout the PBL (up to 19 ppbv) and in the lower free troposphere (Figure 2). The daily aircraft spiral averages were 1.3 DU on 1 April (only one profile measured) and 1.7 DU on 5 April (average of 3 spirals). The operational area average OMI SO_2 values (~2 DU on 1 April and ~3 DU on 5 April) are substantially higher (up to a factor of 2) than average aircraft measurements (Table 2).

[17] One of the reasons for the OMI SO_2 noise and bias is algorithmic assumptions [*Yang et al.*, 2007]. The other reason is imperfect calibration applied to the OMI measured radiance and irradiance data available in the collection 2 level 1b data. Recently level 1b data have been reprocessed (collection 3 data) with several improvements applied to the calibration: (1) daily dark current maps subtracted from the measured radiance and irradiance data and (2) improved radiometric calibration in combination with a modified stray light correction [*Dobber et al.*, 2008]. Preliminary analysis has shown that improved treatment of the dark current has reduced "striping" in residuals. The improved stray light correction is also expected to have a positive effect by reducing the bias in operational SO_2 data. To demonstrate this, we reran the operational OMI SO_2 algorithm using collection 3 OMTO3 residuals without making any changes to the algorithm and software. These results are shown in Table 2 as collection 3 OMI SO_2 data. As can be seen, the SO_2 noise and positive bias on clear days remain the same. However, collection 3 SO_2 data are lower and in better agreement with aircraft measurements (within 15%) on both polluted days.

3.2. Individual Case Comparisons

[18] Comparisons with aircraft measurements for the individual profiling flight patterns (spirals) are summarized in Table 3. To reduce the noise, the OMI IFOV data were averaged within 30 km of each spiral ($n \sim 4$–9) and compared with vertically integrated (up to 4 km) in situ aircraft data. For such small samples, the OMI noise is estimated to be 1.2–1.6 DU (double SDM(n) in Table 1b) depending on the number of IFOV averaged (n), not including a possible AMF error. OMI (collection 2) SO_2 retrievals are larger than the aircraft measurements in all cases. The largest difference of 2.3 DU (150%) is found over Taoxian International Airport on 5 April and the smallest difference (~0.4 DU or 17%) over Liaozhong on the same day (Table 3). In other polluted cases OMI values are doubled compared to the aircraft measurements. On both clean days (7 and 10 April) OMI values are within the noise level. Reprocessing OMI SO_2 data with the operational algorithm, but better calibrated level 1b data (collection 3 data in Table 3) resulted in improved agreement with aircraft measurements for all retrievals on polluted days. The maximal difference over Taoxian International Airport on 5 April is reduced to 1.3 DU (90%), which is comparable to the noise. The differences are smaller in other polluted cases.

[19] Using aircraft SO_2 and aerosol profile data one can partition the total OMI error between AMF error and retrieval error not related to the operational AMF assumptions (equation (2)). To quantify the latter, the operational AMF was corrected to account for known sources of systematic errors. First, the SO_2 cross sections [*Bogumil et al.*, 2003] were corrected using aircraft-measured SO_2 and temperature profiles. For example, the SO_2-weighted temperature over Liaozhong on 5 April was close to 289 K, higher than the PBL temperature of 275 K assumed in the operational OMI algorithm. In this case the assumed differential SO_2 cross sections are overestimated by 4.5% and operational SO_2 values are underestimated by the same percentage. Therefore, the temperature correction resulted in an increase in the operational SO_2 values. Next, the operational AMF was corrected to account for the aircraft-measured SO_2 and aerosol profiles (Figure 7), total ozone, and OMI viewing geometry. The correction was done using a linear regression (equations (5)–(7)), where regression coefficients were recalculated for each spiral using the actual aircraft measured aerosol optical properties and aerosol and SO_2 vertical profiles. The aerosol scattering coefficients were measured in situ at 3 visible wavelengths: 450 nm, 550 nm, and 650 nm and the AOT at 500 nm was estimated assuming a constant value of SSA at 500 nm (0.9). The spectral dependence of the AOT and SSA in the UV was calculated using Mie code (spherical particle assumption) with refractive index and size distributions from OMI dust and industrial aerosol models [*Torres et al.*, 2007]. These parameters, together with the measured SO_2 and aerosol vertical profiles and TOMS climatological ozone vertical profiles, were input to the radiative transfer code to calculate the AMF regression as a function of SCO, for each spiral location (7). The resulting AMF*s* for the Liaozhong spiral on 5 April are shown in Figure 7 for 3 scenarios: no aerosols, industrial aerosols, and dust aerosols. The industrial aerosols with a flat SSA spectral dependence (mixtures of sulfate and black carbon) have little effect on the AMF, while dust aerosols with enhanced UV absorption (dust and secondary organic aerosols (SOA)) would reduce

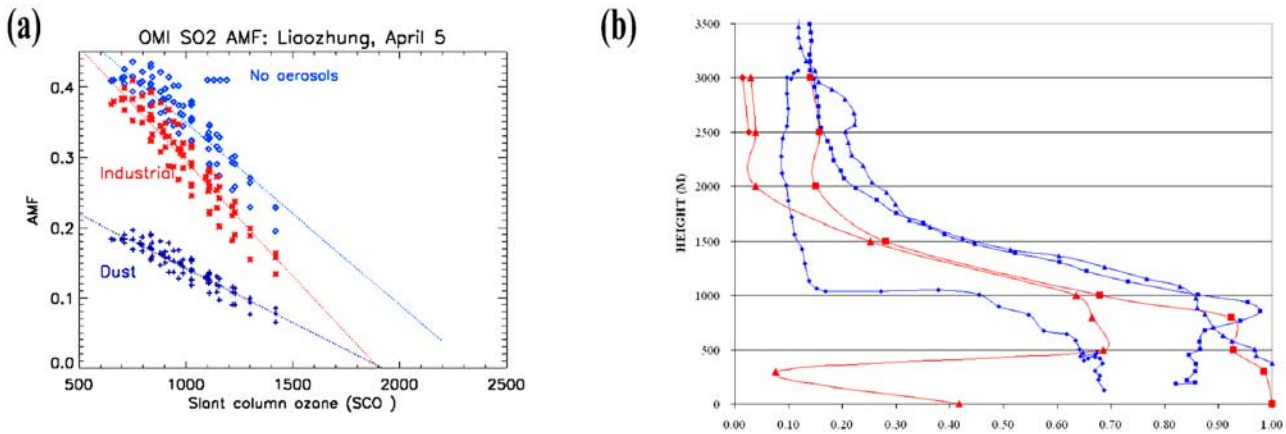

Figure 7. (left) SO_2 AMF parameterization as function of SCO for a 275 DU ozone profile, different viewing and solar zenith angles, solar azimuth 60?120° and 0.05 surface albedo. Blue diamonds, red stars, and purple crosses indicate the aerosol model used in the parameterization, respectively: no aerosols or clouds, an OMI industrial aerosol model (sulfate/soot mixture), and a dust aerosol model with the same optical parameters in the visible wavelengths. (right) Normalized vertical profile of the aerosol scattering coefficient from aircraft in situ measurements (blue lines) and normalized SO_2 concentration profile from aircraft in situ measurements on 5 April (red lines). Symbols indicate spiral location: Xiaoming (triangle), Taoxian (diamond), and Liaozhong (square).

the AMF by half (Figure 7, left). We note that these two types of aerosols have the same optical properties in the visible wavelengths (AOT $\sim$ 1 and SSA $\sim$ 0.9 at 450 nm), where aerosol measurements are typically available, but quite different SSA at the UVB wavelengths ($\sim$310–315 nm) where OMI SO_2 retrievals are done. Assuming only a soot/sulfate mixture would result in an OMI retrieved value of $\sim$2 DU SO_2 in this particular case. However, assuming a dust aerosol regime with the same properties in the visible would result in twice as much SO_2 ($\sim$4–5 DU).

[20] AMF corrections assuming an industrial aerosol model are typically small (<10%) for all polluted cases, except for one case over Taoxian airport on 1 April (Table 3). In this case the combination of high total ozone ($\sim$400 DU) and a large OMI viewing angle (40°) results in a large downward AMF correction, so that the corrected SO_2 value is increased by 50% from 1.4 DU to 2.1 DU. The aircraft measured SO_2 was close to 1.3 DU in this case, so that the AMF adjustment using an industrial aerosol model increases the difference. Using a dust aerosol model would result in an even smaller AMF, which would further increase the difference. We conclude that the OMI collection 3 SCD is still high in this case, which is accidentally compensated by the overestimated value of the operational AMF (0.36; equation (1)). Therefore, making off-line AMF adjustments is important for estimating unbiased errors in the OMI SCD retrievals. Overall, AMF-corrected collection 3 OMI data are higher than aircraft measurements. In polluted cases the bias ranges from 0.2 DU (10%) to 1.2 DU (80%) and on clear days from 0.4 DU to 1 DU. The average positive bias is close to +0.6 DU. This bias is insignificant compared to the noise in the OMI data ($\sim$1.3 DU).

4. Conclusions

[21] In this first OMI SO_2 validation study, conducted over Shenyang in NE China as part of the EAST-AIRE field campaign in April 2005, SO_2 observations from instrumented aircraft flights are compared with OMI operational (collection 2) and reprocessed (collection 3) OMI SO_2 data. Comparisons are made for clear and polluted days under favorable observational conditions (no clouds, near nadir viewing directions). The following conclusions can be drawn:

[22] 1. Operational OMI PBL SO_2 measurements qualitatively agree with the aircraft in situ observations of high SO_2 column amounts (approximately 1–2.DU) ahead of a cold front (1 and 5 April) and lower concentrations behind it (7 and 10 April). This comparison demonstrates that OMI can distinguish between background SO_2 conditions and heavy pollution on a daily basis. This supports the potential application of the OMI PBL SO_2 product to regional air pollution studies.

[23] 2. To evaluate the minimum detectable amount of OMI PBL SO_2 under optimal observational conditions (no clouds, solar zenith angle $\sim$40° and near nadir viewing angles) we examined the signal and its variability over a remote region of the South Pacific where the column content should be consistently well below 0.1 DU. For individual instantaneous field of view (IFOV) data, the standard deviation (σ) is σ = $\sim$1.5 DU. The noise can be reduced by averaging over a larger area or for a longer time. For a single day, σ falls to 0.82 DU for an averaging area with a radius of 20 km (4 IFOV data) and to 0.36 DU for radius of 70 km (44 IFOV data), but increasing the area further has little impact on the noise; for a 100 km radius with 89 IFOV data σ = 0.28. Averaging over 75 days (for each of which at least 70 cloud-free IFOV points were available) for the whole 2° × 2° area gave a standard deviation of 0.6 DU. The variability in the measurement is greater than expected from purely random errors such as instrument noise due, perhaps, to systematic errors such as variability in surface conditions or stratospheric ozone.

[24] 3. A positive bias of up to 150% is demonstrated in the operational collection 2 OMI data (OMI being higher) on polluted days. Reprocessed OMI SO_2 data with better calibrated radiance/irradiance data (collection 3 level 1b data) reduces the difference with aircraft measurements on polluted days, but has little effect on clean days.

[25] 4. The operational SO_2 data were corrected off-line to account for the AMF dependence on total ozone, SO_2 profile, viewing geometry, and aerosol effects. Overall, AMF-corrected collection 3 OMI data are higher than aircraft measurements. In polluted cases the overestimation ranges from 0.2 DU (10%) to 1.2 DU (80%) and on clear days from 0.4 DU to 1 DU. The campaign average OMI bias is close to +0.6 DU.

[26] 5. Absorbing aerosols interfere with OMI SO_2 retrievals by affecting the AMF. The industrial aerosols have little effect on the AMF, while dust aerosols (large particles, with strong absorption in UV) reduce the AMF by half doubling the retrieved SO_2. Therefore quantifying the spectral dependence of aerosol absorption at SO_2 wavelengths (310–330 nm) is critical for accurate retrieval of SO_2 amounts using satellite UV measurements.

[27] **Acknowledgments.** The Dutch-Finnish built OMI instrument is part of the NASA EOS Aura satellite payload. The OMI project is managed by NIVR and KNMI in the Netherlands. The authors would like to thank the KNMI OMI team for producing L1B radiance data and the U.S. OMI operational team for continuing support. Nickolay Krotkov, Russell Dickerson, Arlin Krueger, Simon Carn and Brittany McClure acknowledge NASA funding of OMI SO_2 research and validation (grants NNG06GI00G and NNG06GJ02G); Arlin Krueger, Simon Carn, and Kai Yang acknowledge NASA CAN (NNS06AA05G) funding. Zhanqing Li acknowledges support from the NASA Radiation Science Program (NNG04GE79G) and support for the EAST-AIRE project from UMD CMPS. The aircraft campaign was also supported by NSF. The authors are grateful to Jennifer Hains for help with processing aircraft data and to Colin Seftor for producing OMI/MODIS composite figures. The authors are grateful to Jian Yuan, Fujiu Gong, and X. Bian from Liaoning Provincial Meteorological Bureau, China for help during the EAST-AIRE field campaign.

References

Alfaro, S. C., S. Lafton, J. L. Rajot, P. Formenti, A. Gaudichet, and M. Maille (2004), Iron oxides and light absorption by pure desert dust: An experimental study, *J. Geophys. Res.*, *109*, D08208, doi:10.1029/2003JD004374.

An, X., T. Zhu, Z. Wang, C. Li, and Y. Wang (2007), A modeling analysis of a heavy air pollution episode occurred in Beijing, *Atmos. Chem. Phys.*, *7*, 3103–3114.

Anderson, T. L., and J. A. Ogren (1998), Determining aerosol radiative properties using the TSI 3563 Integrating Nephelometer, *Aerosol Sci. Technol.*, *29*, 57–69, doi:10.1080/02786829808965551.

Anderson, T. L., et al. (1996), Performance characteristics of a high-sensitivity, three-wavelength, total scatter/backscatter nephelometer, *J. Atmos. Oceanic Technol.*, *13*, 967–986, doi:10.1175/1520-0426(1996)013<0967:PCOAHS>2.0.CO;2.

Benkovitz, C. M., S. E. Schwartz, M. P. Jensen, M. A. Miller, R. C. Easter, and T. S. Bates (2004), Modeling atmospheric sulfur over the Northern Hemisphere during the Aerosol Characterization Experiment 2 experimental period, *J. Geophys. Res.*, *109*, D22207, doi:10.1029/2004JD004939.

Bhartia, P. K., and C. W. Wellemeyer (2002), OMI TOMS-V8 total O3 algorithm, *Algorithm Theoretical Basis Document, OMI Ozone Products*, *ATBD-OMI-02,* version 2.0, vol. II, edited by P. K. Bhartia, NASA Goddard Space Flight Cent., Greenbelt, Md. (Available at http://eospso.gsfc.nasa.gov/eos_homepage/for_scientists/atbd/docs/OMI/ATBD-OMI-02.pdf)

Bogumil, K., et al. (2003), Measurements of molecular absorption spectra with the SCIAMACHY pre-flight model: Instrument characterization and reference data for atmospheric remote-sensing in the 230–2380 nm region, *J. Photochem. Photobiol. Chem.*, *157*, 167–184, doi:10.1016/S1010-6030(03)00062-5.

Bovensmann, H., J. P. Burrows, M. Buchwitz, J. Frerick, S. Noël, V. V. Rozanov, K. V. Chance, and A. P. H. Goede (1999), SCIAMACHY: Mission objectives and measurement modes, *J. Atmos. Sci.*, *56*(2), 127–150, doi:10.1175/1520-0469(1999)056<0127:SMOAMM>2.0.CO;2.

Bramstedt, K., A. Richter, M. Van Roozendael, and I. De Smedt (2004), Comparisons of SCIAMACHY sulfur dioxide observations, in *Proceedings of the Second Workshop on the Atmospheric Validation of Envisat (ACVE-2), 3–7 May 2004, Frascati* [CD-ROM], *Eur. Space Agency Spec. Publ.*, *ESA SP-562*.

Burrows, J. P., et al. (1999), The Global Ozone Monitoring Experiment (GOME): Mission concept and first scientific results, *J. Atmos. Sci.*, *56*, 151–175, doi:10.1175/1520-0469(1999)056<0151:TGOMEG>2.0.CO;2.

Carn, S. A., A. J. Krueger, G. J. S. Bluth, S. J. Schaefer, N. A. Krotkov, I. M. Watson, and S. Datta (2003), Volcanic eruption detection by the Total Ozone Mapping Spectrometer (TOMS) instruments: A 22-year record of sulphur dioxide and ash emissions, in *Volcanic Degassing*, edited by C. Oppenheimer, D. M. Pyle, and J. Barclay, *Spec. Publ. Geol. Soc. London*, *213*, 177–202.

Carn, S. A., N. A. Krotkov, M. A. Gray, and A. J. Krueger (2004), Fire at Iraqi sulfur plant emits SO_2 clouds detected by Earth Probe TOMS, *Geophys. Res. Lett.*, *31*, L19105, doi:10.1029/2004GL020719.

Carn, S. A., A. J. Krueger, N. A. Krotkov, K. Yang, and P. F. Levelt (2007), Sulfur dioxide emissions from Peruvian copper smelters detected by the Ozone Monitoring Instrument, *Geophys. Res. Lett.*, *34*, L09801, doi:10.1029/2006GL029020.

Chin, M., et al. (2000), Atmospheric sulfur cycle simulated in the global model GOCART: Comparison with field observations and regional budgets, *J. Geophys. Res.*, *105*(D20), 24,689–24,712, doi:10.1029/2000JD900385.

d'Almeida, G. A., P. Koepke, and E. P. Shettle (1991), *Atmospheric Aerosols: Global Climatology and Radiative Characteristics*, 557 pp., A. Deepak Publ., Hampton, Va.

Dave, J. V. (1964), Meaning of successive iteration of the auxiliary equation of radiative transfer, *Astrophys. J.*, *140*, 1292–1303, doi:10.1086/148024.

Dickerson, R. R., et al. (2007), Aircraft observations of dust and pollutants over northeast China: Insight into the meteorological mechanisms of transport, *J. Geophys. Res.*, *112*, D24S90, doi:10.1029/2007JD008999.

Dobber, M. R., Q. Kleipool, R. Dirksen, P. F. Levelt, G. Jaross, S. Taylor, T. Kelly, and L. Flynn (2008), Validation of Ozone Monitoring Instrument level 1b data products, *J. Geophys. Res.*, *113*, D15S06, doi:10.1029/2007JD008665.

Draxler, R. R., and G. D. Rolph (2003), HYSPLIT (HYbrid Single-Particle Lagrangian Integrated Trajectory) model, NOAA Air Resour. Lab., Silver Spring, Md. (Available at http://www.arl.noaa.gov/ready/hysplit4.html)

Eisinger, M., and J. P. Burrows (1998), Tropospheric sulfur dioxide observed by the ERS-2 GOME instrument, *Geophys. Res. Lett.*, *25*, 4177–4180, doi:10.1029/1998GL900128.

Khokhar, M. F., C. Frankenberg, M. Van Roozendael, S. Beirle, S. Kühl, A. Richter, U. Platt, and T. Wagner (2005), Satellite observations of atmospheric SO_2 from volcanic eruptions during the time-period of 1996–2002, *Adv. Space Res.*, *36*(5), 879–887, doi:10.1016/j.asr.2005.04.114.

King, M. D., W. P. Menzel, Y. J. Kaufman, D. Tanre, B. Gao, S. Platnick, S. A. Ackerman, L. A. Remer, R. Pincus, and P. A. Hubanks (2003), Cloud and aerosol properties, precipitable water, and profiles of temperature and water vapor from MODIS, *IEEE Trans. Geosci. Remote Sens.*, *41*(2), 442–458, doi:10.1109/TGRS.2002.808226.

Krotkov, N. A., S. A. Carn, A. J. Krueger, P. K. Bhartia, and K. Yang (2006), Band residual difference algorithm for retrieval of SO_2 from the Aura Ozone Monitoring Instrument (OMI), *IEEE Trans. Geosci. Remote Sens.*, *44*(5), 1259–1266, doi:10.1109/TGRS.2005.861932.

Krotkov, N., A. Krueger, K. Yang, S. Carn, P. K. Bhartia, and P. Levelt (2007), SO_2 Data from the Ozone Monitoring Instrument (OMI), *Proceedings of the ENVISAT Symposium 2007* [CD-ROM], edited by H. Lacoste and L. Ouwehand, *Eur. Space Agency Spec. Publ.*, *ESA SP-636*.

Krueger, A. J., L. S. Walter, P. K. Bhartia, C. C. Schnetzler, N. A. Krotkov, I. Sprod, and G. J. S. Bluth (1995), Volcanic sulfur dioxide measurements from the total ozone mapping spectrometer instruments, *J. Geophys. Res.*, *100*(D7), 14,057–14,076, doi:10.1029/95JD01222.

Krueger, A. J., S. J. Schaefer, N. Krotkov, G. Bluth, and S. Barker (2000), Ultraviolet remote sensing of volcanic emissions, in *Remote Sensing of Active Volcanism*, *Geophys. Monogr. Ser.*, vol. 116, edited by P. J. Mouginis-Mark, J. A. Crisp, and J. H. Fink, pp. 25–43, AGU, Washington, D. C.

Larssen, T., et al. (2006), Acid rain in China, *Environ. Sci. Technol.*, *40*, 418–425.

Levelt, P. F., G. H. J. van den Oord, M. R. Dobber, A. Mälkki, H. Visser, J. de Vries, P. Stammes, J. Lundell, and H. Saari (2006), The Ozone Monitoring Instrument, *IEEE Trans. Geosci. Remote Sens.*, *44*(5), 1093–1101, doi:10.1109/TGRS.2006.872333.

Li, C., L. T. Marufu, R. R. Dickerson, Z. Li, T. Wen, Y. Wang, P. Wang, H. Chen, and J. W. Stehr (2007), In situ measurements of trace gases

and aerosol optical properties at a rural site in northern China during East Asian Study of Tropospheric Aerosols: An International Regional Experiment 2005, *J. Geophys. Res.*, *112*, D22S04, doi:10.1029/2006JD007592.

Li, Z., et al. (2007), Preface to special section on East Asian Studies of Tropospheric Aerosols: An International Regional Experiment (EAST-AIRE), *J. Geophys. Res.*, *112*, D22S00, doi:10.1029/2007JD008853.

Luke, W. T. (1997), Evaluation of a commercial pulsed fluorescence detector for the measurement of low-level SO_2 concentrations during the Gas-Phase Sulfur Intercomparison Experiment, *J. Geophys. Res.*, *102*, 16,255–16,265, doi:10.1029/96JD03347.

Massie, S. T., O. Torres, and S. J. Smith (2004), Total Ozone Mapping Spectrometer (TOMS) observations increases of Asian aerosol in winter from 1979 to 2000, *J. Geophys. Res.*, *109*, D18211, doi:10.1029/2004JD004620.

McPeters, R. D., G. J. Labow, and J. A. Logan (2007), Ozone climatological profiles for satellite retrieval algorithms, *J. Geophys. Res.*, *112*, D05308, doi:10.1029/2005JD006823.

Mishchenko, M., and I. Geogdzhayev (2007), Satellite remote sensing reveals regional tropospheric aerosol trends, *Opt. Express*, *15*, 7423–7438, doi:10.1364/OE.15.007423.

Ohara, T., H. Akimoto, J. Kurokawa, N. Horii, K. Yamaji, X. Yan, and T. Hayasaka (2007), An Asian emission inventory of anthropogenic emission sources for the period 1980–2020, *Atmos. Chem. Phys.*, *7*, 4419–4444.

Richter, A., F. Wittrock, and J. P. Burrows (2006), SO_2 measurements with SCIAMACHY, in *Proceedings of the Atmospheric Science Conference, 8–12 May 2006, ESRIN, Frascati* [CD-ROM], *Eur. Space Agency Spec. Publ.*, *ESA SP-628*.

Schoeberl, M. R., et al. (2006), Overview of the EOS Aura Mission, *IEEE Trans. Geosci. Rem. Sens.*, *44*(5), 1066–1074, doi:10.1109/TGRS.2005.861950.

Seinfeld, J. H., and S. N. Pandis (1998), *Atmospheric Chemistry and Physics: From Air Pollution to Climate Change*, 1326 pp., John Wiley, New York.

Sokolik, I. N., and O. B. Toon (1999), Incorporation of mineralogical composition into models of the radiative properties of mineral aerosol from UV to IR wavelengths, *J. Geophys. Res.*, *104*(D8), 9423–9444, doi:10.1029/1998JD200048.

Streets, D. G., and S. T. Waldhoff (2000), Present and future emissions of air pollutants in China: SO_2, NO_x, and CO, *Atmos. Environ.*, *34*(3), 363–374, doi:10.1016/S1352-2310 (99)00167-3.

Streets, D. G., et al. (2003), An inventory of gaseous and primary aerosol emissions in Asia in the year 2000, *J. Geophys. Res.*, *108*(D21), 8809, doi:10.1029/2002JD003093.

Taubman, B. F., J. C. Hains, A. M. Thompson, L. T. Marufu, B. G. Doddridge, J. W. Stehr, C. A. Piety, and R. R. Dickerson (2006), Aircraft vertical profiles of trace gas and aerosol pollution over the mid-Atlantic United States: Statistics and meteorological cluster analysis, *J. Geophys. Res.*, *111*, D10S07, doi:10.1029/2005JD006196.

Thomas, W., T. Erbertseder, T. Ruppert, M. Van Roozendael, J. Verdebout, D. Balis, C. Meleti, and C. Zerefos (2005), On the retrieval of volcanic sulfur dioxide emissions from GOME backscatter measurements, *J. Atmos. Chem.*, *50*, 295–320, doi:10.1007/s10874-005-5544-1.

Torres, O., A. Tanskanen, B. Veihelmann, C. Ahn, R. Braak, P. K. Bhartia, P. Veefkind, and P. Levelt (2007), Aerosols and surface UV products from Ozone Monitoring Instrument observations: An overview, *J. Geophys. Res.*, *112*, D24S47, doi:10.1029/2007JD008809.

Yang, K., N. A. Krotkov, A. J. Krueger, S. A. Carn, P. K. Bhartia, and P. F. Levelt (2007), Retrieval of large volcanic SO_2 columns from the Aura Ozone Monitoring Instrument: Comparison and limitations, *J. Geophys. Res.*, *112*, D24S43, doi:10.1029/2007JD008825.

P. K. Bhartia, Laboratory for Atmospheres, NASA Goddard Space Flight Center, Greenbelt, MD 20771, USA.

S. A. Carn and A. J. Krueger, Joint Center for Earth Systems Technology, University of Maryland, Baltimore County, Baltimore, MD 21250, USA.

H. Chen, D. Lu, and P. Wang, Institute of Atmospheric Physics, Chinese Academy of Sciences, Beijing 100021, China.

R. R. Dickerson and B. McClure, Department of Chemistry, University of Maryland, College Park, MD 20742, USA.

N. A. Krotkov and K. Yang, Goddard Earth Sciences and Technology Center, University of Maryland, Baltimore County, Baltimore, MD 21228, USA. (krotkov@mhatter.gsfc.nasa.gov)

P. F. Levelt, Royal Netherlands Meteorological Institute, NL-3730 AE De Bilt, Netherlands.

C. Li and Z. Li, Department of Atmospheric and Oceanic Sciences, University of Maryland, College Park, MD 20742, USA.